

# A two-scale poromechanical model for cohesive rocks

J. Frey · R. Chambon · C. Dascalu

Received: 26 September 2011 / Accepted: 16 April 2012 / Published online: 3 July 2012  
© Springer-Verlag 2012

**Abstract** This paper presents a computational homogenization approach in the framework of poromechanics. A fully coupled hydromechanics problem is formulated at the macroscopic scale. The constitutive equations are replaced by results of numerical computations on a Representative Elementary Volume in order to obtain the overall stress of the mixture as well as its transmissivity properties. At the microscale, the material is assumed to be composed of an assembly of hyperelastic grains connected by cohesive interfaces. These interfaces are also channels of a network where the fluid can percolate. The fluid acts on the boundaries of the grains and influences the behavior of the cohesive interfaces. Conversely, the opening of the interfaces induces changes in the transmissivity properties of the corresponding channels. This yields a fully coupled hydromechanical problem at the microscopic scale. The finite element method is considered for the numerical solutions at both scales, the present approach extending the purely mechanical  $FE^2$  scheme to the coupled hydromechanical framework. The local macroscopic behavior resulting from the homogenization scheme is illustrated on different numerical tests. The results clearly show the coupling between damage and fluid permeability in the

overall response, as a consequence of the small-scale interaction between the action of the percolating fluid, the deformation of the solid skeleton, and the failure of the cohesive interfaces.

**Keywords** Computational homogenization · Geomaterials · Hydromechanical coupling · Multiscale cohesive cracks · Poromechanics · Representative elementary volume

## 1 Introduction

Geomaterials and more specifically rock-like materials have to be studied as multiphase materials. In most engineering problems, the fluid percolating inside the solid skeleton cannot be ignored as it influences the behavior of the mixture. Different approaches can be used to model such media. One is based on mixture theory [6, 9]. Averaging theory [20, 21] is also used, for instance by Lewis and Schrefler [23]. Coussy [8] has developed a general poromechanical theory, generalizing the work of Biot [4] in the framework of the thermodynamics of irreversible processes. In some cases, thermal coupling has also to be considered as in Gatmiri et al. [17], but the present work is restricted to hydromechanical coupling.

For multiphase problems, the governing equations consist of the balance equations (balance of momentum, balance of mass, and also balance of energy if thermal effects are important and cannot be decoupled) and the constitutive equations. If we assume that there are no phase changes, the balance equations have to be written for every phase. Constitutive equations describing the behavior of the different phases and the interactions between phases have to be given. Contrary to the balance equations that are

---

J. Frey  
ANDRA, 1/7, rue Jean Monnet, Parc de la Croix-Blanche,  
92298 Chatenay-Malabry Cedex, France

J. Frey (✉) · R. Chambon  
Laboratoire 3S-R Grenoble, Institut National Polytechnique,  
C.N.R.S. U.M.R. 5521, Université Joseph Fourier,  
B.P. 53X, 38041 Grenoble Cedex, France  
e-mail: jeremy.frey@orange.fr

C. Dascalu  
Institut Jean Le Rond d'Alembert, CNRS, UMR 7190,  
UPMC Univ Paris 06, 75005 Paris, France

well established, the constitutive equations for mixtures are not easy to provide. Their structure can be assumed by phenomenological considerations, and the parameters of these constitutive equations can be obtained using experimental data. Another way to obtain the constitutive equations is the use of homogenization techniques. When only linear constitutive relations are assumed at the microscale, the homogenization techniques represent a powerful tool for obtaining overall responses of materials. However, when non-linear phenomena are involved, homogenization techniques are more difficult to use even if many authors have obtained interesting results. See for instance the work of Dormieux and Kondo [10].

An alternative method to the above-mentioned analytical or semi-analytical homogenization techniques is the numerical homogenization. When finite elements are used at both small and large scales, the method is sometimes called  $FE^2$ . It has been used extensively for mono phasic heterogeneous materials. It consists of numerical computations at the level of the representative elementary volumes (R.E.V.), by considering balance equations and constitutive equations at the microscale. Such studies started in the 90's in the framework of elastic materials [18]. Then, nonlinearity has been taken account and the method has been extended to deal with elastoplasticity [19], viscoelasticity [30], finite plasticity [24], damage [26], and elastoviscoplasticity [14]. More recently, the method has been extended to higher order models [22] and to coupled thermo-mechanical behavior [27]. Preliminary results on the application of the  $FE^2$  method to hydro mechanical problems have been presented in [16].

This paper is a generalization of the  $FE^2$  method for a two phase material. The studied geomaterial consists of an assembly of grains filled with a percolating fluid. The material is assumed to be saturated and only quasi-static problems are studied. It is assumed that all inertia terms are negligible, contrary to what is done for instance in [2] and [5] to obtain a non-conventional Darcy law. Neglecting the inertia terms is a common assumption necessary to obtain the classical Darcy's law. Assuming a steady state at the micro level means that it is assumed that changes are instantaneous which is consistent with the small size of the R.E.V. This assumption is similar to the one done by Ozdemir et al. [27] for thermomechanical problems. Thermal effects are also neglected, only hydro mechanical coupling is taken into account. In this paper, we consider two-dimensional problems and the  $FE^2$  method is developed for this case. For the modelling of some specific physical situations, extension of the present model to 3D framework would be important. This is certainly beyond the scope of the present contribution.

Analytical homogenization techniques, like the self-consistent method (e.g. Dormieux and Kondo [11]), may be

used for the description of damage of saturated poroelastic media. The numerical homogenization scheme presented in this paper has the capacity of modeling complex behaviors such as mass flow evolution for unloading or partially broken or closed interfaces. The given examples are just preliminary results used to show the possibility of such an approach. For application to geotechnical structures, the microstructure must be chosen in agreement with the particular material to be modeled. Obviously, the parameters of the microstructure (geometry, number of interfaces, and properties) will influence the homogenized response.

The presentation is structured as follows. In the first part, the equations of the mixture are written at the macroscale. The unknowns are the positions of the solid skeleton and the pressure of the fluid. The equations are written in the deformed configuration of the solid in order to be able to deal with geometrical nonlinearities. The finite element method used to solve the problem at the macroscale is then described. Time discretization is considered and a full Newton method is used in order to solve the non-linear equations corresponding to a given time step. This allows us to exhibit the quantities needed for the effective response at every macroscopic Gauss point. Usually, they are obtained by integrating the constitutive equations using a so-called stress point algorithm. In the  $FE^2$  method, this effective response results from finite element computations on the R.E.V.

In a second part, the constitutive relations adopted at the microscale are detailed. Elastic grains separated by cohesive interfaces are the elements of the solid skeleton. A compressible fluid is assumed to percolate through the interfaces and to fill all the pores of the solid skeleton. The opening of the cohesive interfaces influences the fluid fluxes and, conversely, normal and tangential fluid forces acting on the grains contribute to the deformation of the skeleton. The periodicity conditions are formulated on the boundary of the R.E.V. The numerical procedure for the micro-macro computations is described. At the microscopic scale, the equations are written in the deformed configuration in order to deal with possible geometrical nonlinearities. This part is a generalization to hydro mechanical problems of the work of Bilbie et al. [3] concerning only dry materials.

Some examples illustrating the influence of the coupling between the solid skeleton and the filtrating fluid are given in a third part, for relatively simple R.E.V. geometries. They show the link between damage and permeability in the homogenized response.

Concerning the notations adopted in the paper, a component of a tensor (or vector) is denoted by the name of the tensor (or vector) accompanied by the indices. All tensorial indices are in lower position, since there is no need in this work to distinguish between covariant and contravariant

components. Upper indices have specific meanings defined in the text. The summation convention with respect to repeated tensorial indices is used. A dot written above a symbol indicates the time derivative. Specific notations are used in the part dealing with the microscale problem.

## 2 Poromechanics formulation at the macroscopic scale

### 2.1 Balance equations

At the macroscopic scale, we consider the classical framework of continuous poromechanics. A mixture of a solid skeleton saturated by a fluid is studied. Inertia forces are assumed to be negligible, so that the quasi-static assumption is adopted. It is well known that in order to model such a mixture, it is necessary to enforce two momentum balance equations and two mass conservation equations.

A current way to do this is to develop in a weak form the balance equation for the whole mixture and the conservation of the fluid mass. The mass conservation of the solid is considered by following the skeleton during the movement. The balance equation for the fluid is usually written in a strong form. It involves the drag forces constitutively given as a function of the velocity of the fluid with respect to the solid skeleton. This is an other way to write the Darcy's law, see for instance [7]. Within the two-scale approach, the balance equation for the fluid does not require any development at the macroscopic scale, it will be satisfied at the microstructure level.

An updated lagrangian method is used and the equations at the macroscopic level are written using the current configuration of the solid skeleton denoted  $\Omega^t$ .

The constitutive equation of the skeleton, of the fluid and the mechanical interaction between the skeleton and the fluid are obtained as consequences of the modeling at the level of the R.E.V.

#### 2.1.1 Balance equation for the mixture

For any kinematically admissible field  $u_i^\star$ :

$$\int_{\Omega^t} \sigma_{ij}^t \frac{\partial u_i^\star}{\partial x_j^t} d\Omega^t = \int_{\Omega^t} \varrho^{\text{mix},t} g_i u_i^\star d\Omega^t + \int_{\Gamma_\sigma^t} \bar{t}_i u_i^\star d\Gamma^t, \quad (1)$$

where  $\sigma_{ij}^t$  is the Cauchy stress of the mixture for a given time  $t$ ,  $\varrho^{\text{mix},t}$  denotes the mass of the mixture per unit current volume,  $\Gamma_\sigma^t$  is the part of the boundary where surface tractions are prescribed and  $\bar{t}_i$  the corresponding prescribed values. This equation is equivalent to the one written in a differential form:

$$\frac{\partial \sigma_{ij}^t}{\partial x_j^t} + \varrho^{\text{mix},t} g_i = 0, \quad (2)$$

for any point in  $\Omega^t$ , and the boundary conditions:

$$\sigma_{ij}^t n_j^t = \bar{t}_i^t, \quad (3)$$

for any point in  $\Gamma_\sigma^t$ , where  $n_j^t$  is the normal to the boundary and  $g_i$  the components of the gravity.

#### 2.1.2 Mass conservation for the fluid

As seen above, due to the choice done, it is only necessary to write the mass conservation for the fluid. Classically, this reads:

$$\dot{M}^t + \frac{\partial m_i^t}{\partial x_i^t} = 0, \quad (4)$$

where  $M^t$  is the fluid mass per unit current volume and  $m_i^t$  is the fluid mass flow.

In order to obtain a weak form of these equations, an admissible (vanishing on the part denoted  $\Gamma_p^t$  of the boundary where the pressure is prescribed) “virtual” field  $p^\star$  is used.

$$\int_{\Omega^t} \left( \dot{M}^t + \frac{\partial m_i^t}{\partial x_i^t} \right) p^\star d\Omega^t = 0. \quad (5)$$

Since

$$\frac{\partial}{\partial x_i^t} (p^\star m_i^t) = p^\star \frac{\partial m_i^t}{\partial x_i^t} + m_i^t \frac{\partial p^\star}{\partial x_i^t}, \quad (6)$$

then

$$\int_{\Omega^t} \left( \dot{M}^t p^\star - m_i^t \frac{\partial p^\star}{\partial x_i^t} \right) d\Omega^t = - \int_{\Gamma_q^t} \bar{q}^t p^\star d\Gamma^t, \quad (7)$$

where

$$\bar{q}^t = m_i^t n_i^t \quad (8)$$

is prescribed on  $\Gamma_q^t$ . Here  $\Gamma^t = \Gamma_p^t \cup \Gamma_q^t$  and  $\Gamma_p^t \cap \Gamma_q^t = \emptyset$ .

### 2.2 Linearization of the field equations

Considering a body subjected to a given loading history of the boundary conditions, the aim is to find the unknown fields  $u_i$ , and  $p$ , which fulfill Eqs. (1) and (7) and the boundary conditions at any time  $t$ . In order to solve this non-linear problem numerically, the loading process is discretized into finite time steps  $\Delta t$ . The system of equations is enforced at the end of each time step. This is achieved by the use of a Newton–Raphson procedure. It is then necessary to define a corresponding linear auxiliary problem.

Assuming known the configuration  $\Omega^t$  at time  $t$  for which all the previous equations are verified, the objective is to find the new configuration at time  $t + \Delta t$ . A first guess of the solutions gives us  $\Omega^{\tau 1}(\tau 1 = t + \Delta t)$  at which the equilibrium is not fulfilled and residual terms appear in the following equations:

$$\int_{\Omega^{\tau 1}} \sigma_{ij}^{\tau 1} \frac{\partial u_i^*}{\partial x_j^{\tau 1}} d\Omega^{\tau 1} - \int_{\Omega^{\tau 1}} \varrho^{\text{mix}, \tau 1} g_i u_i^* d\Omega^{\tau 1} - \int_{\Gamma^{\tau 1}} \bar{t}_i u_i^* d\Gamma^{\tau 1} = R^{\tau 1}, \quad (9)$$

$$\int_{\Omega^{\tau 1}} \left( \dot{M}^{\tau 1} p^* - m_i^{\tau 1} \frac{\partial p^*}{\partial x_i^{\tau 1}} \right) d\Omega^{\tau 1} + \int_{\Gamma_q^{\tau 1}} \bar{q}^{\tau 1} p^* d\Gamma^{\tau 1} = W^{\tau 1}. \quad (10)$$

The aim is now to find a new configuration  $\Omega^{\tau 2}$ , close to  $\Omega^{\tau 1}$ , for which the residuals  $R^{\tau 2}$ ,  $S^{\tau 2}$  and  $W^{\tau 2}$  vanish. In order to get the linear auxiliary problem, the field equations corresponding to  $\Omega^{\tau 2}$  are written on the configuration  $\Omega^{\tau 1}$  and the obtained equations are combined with the Eqs. 9–10. This yields:

$$\int_{\Omega^{\tau 1}} \frac{\partial u_i^*}{\partial x_j^{\tau 1}} \left( \sigma_{ij}^{\tau 2} \frac{\partial x_j^{\tau 1}}{\partial x_j^{\tau 2}} \det F - \sigma_{il}^{\tau 1} \right) d\Omega^{\tau 1} - \int_{\Omega^{\tau 1}} u_i^* (\varrho^{\text{mix}, \tau 2} \det F - \varrho^{\text{mix}, \tau 1}) g_i d\Omega^{\tau 1} = -R^{\tau 1}, \quad (11)$$

$$\int_{\Omega^{\tau 1}} (\dot{M}^{\tau 2} \det F - \dot{M}^{\tau 1}) p^* - \frac{\partial p^*}{\partial x_i^{\tau 1}} \left( m_i^{\tau 2} \frac{\partial x_i^{\tau 1}}{\partial x_i^{\tau 2}} \det F - m_i^{\tau 1} \right) d\Omega^{\tau 1} = -W^{\tau 1}. \quad (12)$$

where we have assumed that  $g_i$ ,  $\bar{t}_i$  and  $\bar{q}$  are position independent. Here  $\det F$  is the Jacobian of  $F_{ij} = \partial x_i^{\tau 2} / \partial x_j^{\tau 1}$ .

Let us introduce the following definitions:

$$\delta u_j = x_j^{\tau 2} - x_j^{\tau 1} \quad \delta \sigma_{il} = \sigma_{il}^{\tau 2} - \sigma_{il}^{\tau 1} \quad \delta p = p^{\tau 2} - p^{\tau 1} \quad \delta \rho^{\text{mix}} = \rho^{\text{mix}, \tau 2} - \rho^{\text{mix}, \tau 1}. \quad (13)$$

Using a Taylor expansion and discarding terms of degrees greater than one we get, after some algebra, the linearized equations that allow us to find the correction of the displacement field  $\delta u_i$  and the corrections of the pressure  $\delta p$  to be added to their respective current values in order to define a new current configuration. The process is then iterated until convergence. When convergence is obtained Eqs. (1) and (7) are well balanced.

The linearized equations are:

$$\int_{\Omega^{\tau 1}} \frac{\partial u_i^*}{\partial x_j^{\tau 1}} \left( \delta \sigma_{il} - \sigma_{ij}^{\tau 1} \frac{\partial \delta u_l}{\partial x_j^{\tau 1}} + \sigma_{il}^{\tau 1} \frac{\partial \delta u_m}{\partial x_m^{\tau 1}} \right) d\Omega^{\tau 1} - \int_{\Omega^{\tau 1}} u_i^* \left[ \varrho^{\text{mix}, \tau 1} \frac{\partial \delta u_m}{\partial x_m^{\tau 1}} - \delta \varrho^{\text{mix}} \right] g_i d\Omega^{\tau 1} = -R^{\tau 1}, \quad (14)$$

$$\int_{\Omega^{\tau 1}} p^* \left( \delta \dot{M} + \dot{M}^{\tau 1} \frac{\partial \delta u_m}{\partial x_m^{\tau 1}} \right) d\Omega^{\tau 1} - \int_{\Omega^{\tau 1}} \frac{\partial p^*}{\partial x_j^{\tau 1}} \left( \delta m_l - m_l^{\tau 1} \frac{\partial \delta u_l}{\partial x_j^{\tau 1}} + m_l^{\tau 1} \frac{\partial \delta u_m}{\partial x_m^{\tau 1}} \right) d\Omega^{\tau 1} = -W^{\tau 1}, \quad (15)$$

where  $\sigma_{il}$ ,  $\varrho^{\text{mix}}$ ,  $\dot{M}$  and  $m_i$  are usually coming from constitutive equations of the mixture. In this paper, a computation at the micro level gives us the numerical values of all these functions.

A consistent linearization of the constitutive equations of the mixture yields:

$$\delta \sigma_{il} = C_{ilkj} \frac{\partial \delta u_k^{\tau 1}}{\partial x_j^{\tau 1}} + A_{il} \delta p + B_{ilj} \frac{\partial \delta p}{\partial x_j^{\tau 1}}, \quad (16)$$

$$\delta \varrho^{\text{mix}} = D_{ij} \frac{\partial \delta u_i^{\tau 1}}{\partial x_j^{\tau 1}} + E \delta p + G_k \frac{\partial \delta p}{\partial x_k^{\tau 1}}, \quad (17)$$

$$\delta \dot{M} = H_{ij} \frac{\partial \delta u_i^{\tau 1}}{\partial x_j^{\tau 1}} + I \delta p + J_k \frac{\partial \delta p}{\partial x_k^{\tau 1}}, \quad (18)$$

$$\delta m_i = K_{ijk} \frac{\partial \delta u_j^{\tau 1}}{\partial x_k^{\tau 1}} + L_i \delta p + Q_{ik} \frac{\partial \delta p}{\partial x_k^{\tau 1}}. \quad (19)$$

In order to simplify the Eqs. (14)–(15), Eqs. (16)–(19) are rewritten as:

$$\delta \sigma_{il} - \sigma_{ij}^{\tau 1} \frac{\partial \delta u_l}{\partial x_j^{\tau 1}} + \sigma_{il}^{\tau 1} \frac{\partial \delta u_m}{\partial x_m^{\tau 1}} = C'_{ilkj} \frac{\partial \delta u_k^{\tau 1}}{\partial x_j^{\tau 1}} + A_{il} \delta p + B_{ilj} \frac{\partial \delta p}{\partial x_j^{\tau 1}}, \quad (20)$$

$$\delta \varrho^{\text{mix}} - \varrho^{\text{mix}, \tau 1} \frac{\partial \delta u_m}{\partial x_m^{\tau 1}} = D'_{ij} \frac{\partial \delta u_i^{\tau 1}}{\partial x_j^{\tau 1}} + E \delta p + G_k \frac{\partial \delta p}{\partial x_k^{\tau 1}}, \quad (21)$$

$$\delta \dot{M} + \dot{M}^{\tau 1} \frac{\partial \delta u_m}{\partial x_m^{\tau 1}} = H'_{ij} \frac{\partial \delta u_i^{\tau 1}}{\partial x_j^{\tau 1}} + I \delta p + J_k \frac{\partial \delta p}{\partial x_k^{\tau 1}}, \quad (22)$$

$$\delta m_l - m_l^{\tau 1} \frac{\partial \delta u_l}{\partial x_i^{\tau 1}} + m_l^{\tau 1} \frac{\partial \delta u_m}{\partial x_m^{\tau 1}} = K'_{ijk} \frac{\partial \delta u_j^{\tau 1}}{\partial x_k^{\tau 1}} + L_i \delta p + Q_{ik} \frac{\partial \delta p}{\partial x_k^{\tau 1}}. \quad (23)$$

Finally, the computation at the microscale has to give us  $\sigma_{il}$ ,  $\varrho^{\text{mix}}$ ,  $\dot{M}$  and  $m_i$ ,  $C_{ilkj}$ ,  $A_{il}$ ,  $B_{ilj}$ ,  $D_{ij}$ ,  $E$ ,  $G_k$ ,  $H_{ij}$ ,  $I$ ,  $J_k$ ,  $K_{ijk}$ ,  $L_i$ , and  $Q_{ik}$ . In fact, the values of  $\varrho^{\text{mix}}$  and  $\dot{M}$  are dependent, but it is simpler to use both quantities in the developments done above.

### 2.3 Coupled finite element formulation

In the following, a two-dimensional problem is assumed.

The field Eqs. (14)–(15) are supposed to be spatially discretized using 2D plane strain isoparametric finite elements with eight nodes for  $u_i$  and  $p$ . The usual quadratic serendipity shape function are used for  $u_i$  and  $p$ .

It can also be chosen to use quadratic shape functions for the displacements but linear shape functions for the pressure as it has been done by Andrade and Borja [1] to avoid locking. However, in our case, the fluid is assumed to be compressible and it is not sure that the behavior of the skeleton induces a kinematical constraint similar to a flow rule. Numerical experiments have to be performed to clarify this point. Nevertheless, it has been proved by Ern and Meunier [12] that if the polynomial interpolation for the displacement is one degree higher than for the pressure, the convergence of the numerical method of the linear poroelasticity problem is optimal. A comparison of the two possible choices should then be addressed in the future for our problem.

In order to define the local element stiffness matrix, Eqs. (14)–(15) are rewritten in a matricial form:

$$\int_{\Omega^{\tau 1}} [U_{(x,y)}^{*,\tau 1}]^T [E^{\tau 1}] [\delta U_{(x,y)}^{\tau 1}] d\Omega^{\tau 1} = -R^{\tau 1} - W^{\tau 1}, \quad (24)$$

where  $[\delta U_{(x,y)}^{\tau 1}]$  is defined in Eq. (25) and  $[U_{(x,y)}^{*,\tau 1}]$  has the same composition with corresponding virtual quantities.  $[A]^T$  means the transpose of matrix  $[A]$ .

$$[\delta U_{(x,y)}^{\tau 1}] \equiv \left[ \frac{\partial \delta u_1^{\tau 1}}{\partial x_1^{\tau 1}} \frac{\partial \delta u_1^{\tau 1}}{\partial x_2^{\tau 1}} \frac{\partial \delta u_2^{\tau 1}}{\partial x_1^{\tau 1}} \frac{\partial \delta u_2^{\tau 1}}{\partial x_2^{\tau 1}} \delta u_1^{\tau 1} \delta u_2^{\tau 1} \frac{\partial \delta p^{\tau 1}}{\partial x_1^{\tau 1}} \frac{\partial \delta p^{\tau 1}}{\partial x_2^{\tau 1}} \delta p^{\tau 1} \right]. \quad (25)$$

The FE spatial discretization is introduced in Eq. (24) using the transformation matrices  $[T^{\tau 1}]$  and  $[B]$ , which connect  $[\delta U_{(x,y)}^{\tau 1}]$  to the nodal variables:

$$[\delta U_{(x,y)}^{\tau 1}] = [T^{\tau 1}] [\delta U_{(\xi,\eta)}^{\tau 1}] \quad (26)$$

and

$$[\delta U_{(\xi,\eta)}^{\tau 1}] = [B] [\delta U_{\text{Node}}^{\tau 1}]. \quad (27)$$

Integration of Eq. (24) on the finite element volume then yields:

$$[U_{\text{Node}}^*]^T \int_{-1}^1 \int_{-1}^1 [B]^T [T^{\tau 1}]^T [E^{\tau 1}] [T^{\tau 1}] [B] \det J^{\tau 1} d\xi d\eta [\delta U_{\text{Node}}^{\tau 1}] \equiv [U_{\text{Node}}^*]^T [k^{\tau 1}] [\delta U_{\text{Node}}^{\tau 1}], \quad (28)$$

where  $[k^{\tau 1}]$  is the local element stiffness matrix,  $J^{\tau 1}$  is the Jacobian matrix of the mapping from the  $(\xi, \eta)$  space to the  $(x, y)$  one and  $[\delta U_{\text{Node}}^{\tau 1}]$  has the following definition:

$$[\delta U_{\text{Node}}^{\tau 1}]^T = \left[ \delta u_1^{\tau 1}(-1,-1) \delta u_2^{\tau 1}(-1,-1) \delta p^{\tau 1}(-1,-1) \delta u_1^{\tau 1}(-1,0) \delta u_2^{\tau 1}(-1,0) \delta p^{\tau 1}(-1,0) \delta u_1^{\tau 1}(-1,1) \delta u_2^{\tau 1}(-1,1) \delta p^{\tau 1}(-1,1) \delta u_1^{\tau 1}(0,-1) \delta u_2^{\tau 1}(0,-1) \delta p^{\tau 1}(0,-1) \delta u_1^{\tau 1}(0,0) \delta u_2^{\tau 1}(0,0) \delta p^{\tau 1}(0,0) \delta u_1^{\tau 1}(0,1) \delta u_2^{\tau 1}(0,1) \delta p^{\tau 1}(0,1) \delta u_1^{\tau 1}(1,-1) \delta u_2^{\tau 1}(1,-1) \delta p^{\tau 1}(1,-1) \delta u_1^{\tau 1}(1,0) \delta u_2^{\tau 1}(1,0) \delta p^{\tau 1}(1,0) \delta u_1^{\tau 1}(1,1) \delta u_2^{\tau 1}(1,1) \delta p^{\tau 1}(1,1) \right]. \quad (29)$$

$[E^{\tau 1}]$  is a  $9 \times 9$  matrix that contains all the terms of Eqs. 20–23:

$$[E^{\tau 1}] = \begin{bmatrix} C'_{1111} & C'_{1112} & C'_{1121} & C'_{1122} & 0 & 0 & B_{111} & B_{112} & A_{11} \\ C'_{1211} & C'_{1212} & C'_{1221} & C'_{1222} & 0 & 0 & B_{121} & B_{122} & A_{12} \\ C'_{2111} & C'_{2112} & C'_{2121} & C'_{2122} & 0 & 0 & B_{211} & B_{212} & A_{21} \\ C'_{2211} & C'_{2212} & C'_{2221} & C'_{2222} & 0 & 0 & B_{221} & B_{222} & A_{22} \\ D'_{11g1} & D'_{12g1} & D'_{21g1} & D'_{22g1} & 0 & 0 & G_{1g1} & G_{2g1} & E_{g1} \\ D'_{11g2} & D'_{12g2} & D'_{21g2} & D'_{22g2} & 0 & 0 & G_{1g2} & G_{2g2} & E_{g2} \\ K'_{111} & K'_{112} & K'_{121} & K'_{122} & 0 & 0 & Q_{11} & Q_{12} & L_1 \\ K'_{211} & K'_{212} & K'_{221} & K'_{222} & 0 & 0 & Q_{21} & Q_{22} & L_2 \\ H'_{11} & H'_{12} & H'_{21} & H'_{22} & 0 & 0 & J_1 & J_2 & I \end{bmatrix}. \quad (30)$$

The residual of Eq. (24),  $R^{\tau 1}$  and  $W^{\tau 1}$  are computed for each element using the following relationships:

$$-R^{\tau 1} - W^{\tau 1} = P_e^{*} - [U_{\text{Node}}^*]^T \int_{-1}^1 \int_{-1}^1 [B]^T [T^{\tau 1}]^T [\sigma^{\tau 1}] \times \det J^{\tau 1} d\xi d\eta \equiv [U_{\text{Node}}^*] [\delta f_{\text{HE}}^{\tau 1}], \quad (31)$$

$$[\sigma^{\tau 1}] = [\sigma_{11}^{\tau 1} \sigma_{12}^{\tau 1} \sigma_{21}^{\tau 1} \sigma_{22}^{\tau 1} - q^{\text{mix},\tau 1} g_1 - q^{\text{mix},\tau 1} g_2 - m_1^{\tau 1} - m_2^{\tau 1} \dot{M}^{\tau 1}], \quad (32)$$

where  $[\delta f_{\text{HE}}^{\tau 1}]$  are the elementary out-of-balance forces. The external virtual power  $P_e^{*}$  corresponds to the boundary values (for the mechanical and flow problem), except the term related to gravity volume force, which is introduced in the  $[\sigma^{\tau 1}]$  vector.

### 2.4 Time evolution assumption

We just described the spatial discretization of the problem with the finite element method for a given time, assumed to be the end of a time step. However, the flow diffusion equation is time dependent. A finite difference scheme is then used to define the temporal evolution during a finite time step and the time derivatives:

$$\begin{aligned} t &= (1 - \theta)t^t + \theta t^{t+\Delta t}, \\ x_i &= (1 - \theta)x_i^t + \theta x_i^{t+\Delta t}, \\ \frac{\partial p}{\partial t} &= \frac{p^{t+\Delta t} - p^t}{t^{t+\Delta t} - t^t} = \frac{\Delta p}{\Delta t}, \end{aligned} \quad (33)$$



$$\dot{p}^{t+\Delta t} = \frac{p^{t+\Delta t} - p^t}{\Delta t}. \quad (34)$$

Knowing the time evolution of all the nodal variables, the field equations have to be met during the entire time step. A weighted residual method in time with point collocation is used here. The choice of the  $\theta$  value is not trivial, it is possible to show, for linear systems, that the problem is unconditionally stable for  $\theta \geq 0.5$ . However, the system of equations considered here is highly non-linear and there is no proof that the previous conclusion is still valid in this case. The practice shows that extrapolations to the non-linear cases of the conclusions obtained for the linear case are generally good enough. In our computation, a fully implicit scheme is chosen ( $\theta = 1$ ).

The global stiffness matrix and the out-of-balance force can be obtained by assembling the elementary matrices given by Eqs. (28) and (31). After solving the resulting auxiliary linear system, a new configuration is found and the equilibrium is checked. Other approaches exist to solve coupled equations problems. The staggered procedure consists in solving a first block of equations related to a variable field while the other is kept constant. In a second step, the second block of equations is solved in order to find the other variable while the previous updated variable remains fixed (see [13, 23] and [28] for instance). Here, a monolithic procedure is chosen where the full stiffness matrix is computed for each iteration of the Newtown-Raphson procedure.

### 3 Model at the microscale

#### 3.1 Macroscopic FEM input and output for the REV

At the end of Sect. 2.2, the values needed by the macro-scale finite element algorithm have been summarized.  $C_{ilkj}$ ,  $A_{il}$ ,  $B_{ilj}$ ,  $D_{ij}$ ,  $E$ ,  $G_k$ ,  $H_{ij}$ ,  $I$ ,  $J_k$ ,  $K_{ijk}$ ,  $L_i$  and  $Q_{ik}$  are the result of a consistent linearization of the constitutive equation of the mixture used for a finite time step, following the pioneering ideas of Simo [29] for elastoplasticity. Clearly, here, no full analytical method can be used since the constitutive equation is not explicit. Consequently, the consistent linearization is obtained by numerical derivation. The stress point algorithm is performed for the loading path coming from the macroscale computation and also for 7 other loading paths close to the previous one corresponding to small perturbations of one input data (in the case of plane problems). All the tensors recalled above namely  $C_{ilkj}$ ,  $A_{il}$ ,  $B_{ilj}$ ,  $D_{ij}$ ,  $E$ ,  $G_k$ ,  $H_{ij}$ ,  $I$ ,  $J_k$ ,  $K_{ijk}$ ,  $L_i$ ,  $Q_{ik}$  are then computed by finite differences.

For classical monophasic problems, only the description of the kinematics of the time step is necessary to use the

constitutive equation. According to poromechanics, it is necessary to know the pore pressure to obtain the response of the mixture. Moreover, since we use a fully coupled finite element method at the macroscale, the transmissivity properties and the gradient of the pressure are also needed.

Finally, the input data for the REV computations are the kinematics, the pore pressure, and its gradient. This explains, in the 2-D case studied in this paper, why 7 other computations are necessary to obtain the consistent constitutive matrices. We need 4 components for the kinematics description, 1 value for the pressure and 2 for its gradient. The results of the computation of the REV for a loading path are  $\sigma_{il}$ ,  $q^{\text{mix}}$ ,  $\dot{M}$  and  $m_i$  (remember that  $q^{\text{mix}}$  and  $\dot{M}$  are not independent, see Sect. 2.2).

#### 3.2 Assumptions to define the REV

Our model concerns the behavior of cohesive granular rocks. In order to describe real deformation processes at the small scale, we choose a large deformations approach. Such an assumption is appropriate due to the presence of cohesive interfaces. Even if at the scale of the macro-structure, the small deformation framework may be reasonably used for geomaterials as a simpler approximation of the general large deformation framework of continuum mechanics, for two-scale models with microscopic cohesive interfaces large deformations may occur at the small scale and the general model of arbitrary deformations is necessary for a proper description.

##### 3.2.1 Solid phase

We make the following assumptions to define the REV as a compromise between simplicity and physical relevance. It is assumed that the REV is a mixture of solid and fluid phases (see Fig. 1). The dashed lines are the boundaries of the R.E.V., whereas the solid lines are the boundaries of the grains. These boundaries are geometrically periodic. The grains are governed by large strain elastic constitutive equations, whereas cohesive crack models are assumed at interfaces between grains, as already studied by Bilbie et al. [3] in the purely mechanical case. All common boundaries between grains (for instance  $CB$  or  $DE$  in Fig. 1) are assumed to be cohesive interfaces.

##### 3.2.2 Fluid phase

The fluid phase is modeled as channels corresponding with the interfaces between the solid grains. These channels are connected through voids (some voids can have a vanishing volume like points  $A$  or  $B$ , others can have a finite volume like the colored area  $DCFG$  in Fig. 1). Such a model may

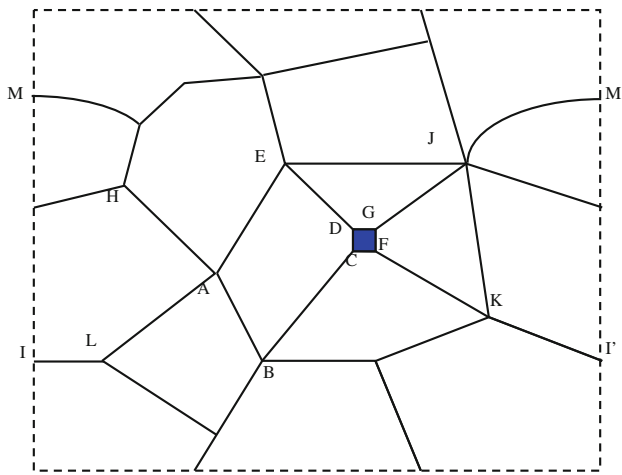


**Fig. 1** The Representative Elementary Volume, (R.E.V.)

be appropriate for the description of the behavior of low-porosity rocks. An alternative choice would have been to solve the Stokes equations in the fluid part of the domain, as it was done for instance in Borne et al. [5]. It is assumed in what follows that all the channels belong to a unique fluid network, as a simplifying assumption for avoiding isolated fluid mass.

According to our assumption, we need for every point of a channel a mass density (per unit volume) denoted  $\varrho$ , a fluid mass per unit length of channel denoted  $v$ , a mass flux denoted  $\overline{w}$  and a pressure denoted  $p$ .

For every connection, void a mass density per unit volume  $\varrho$ , an internal fluid mass  $\mu$ , and a pressure  $p$  are used. This implies that the connections are small enough to assume a constant pressure. Let us remark that  $\mu$  is depending on the local opening of the connection void if it is not assumed to have a negligible volume.

### 3.3 Mass balance equations

Since we perform an updated Lagrangian computation following the solid phase, the mass balance equation of the solid is then necessarily verified.

At the microscale for the fluid, the quasi-static evolution assumption means that we are dealing with steady state flows. There are two different kinds of mass balance equations. The first one corresponding to a given channel reads:

$$\frac{d\overline{w}}{ds} = 0, \quad (35)$$

where  $s$  is the coordinate along the channel. Finally,  $\overline{w}$  is constant all along each channel.

The second one correspond to the connection, it reads:

$$\dot{\mu} = \sum_{\text{channels}} \overline{w}. \quad (36)$$

In the case of a connection with a negligible volume  $\dot{\mu} = 0$ .

### 3.4 Balance of momentum equations

The balance of momentum equation for the solid is written in the same manner as in Bilbie et al. [3] except that forces due to the percolating fluid are prescribed on the boundaries of the grains. Along the interfaces, both normal (pressure) and tangential forces are taken into account whereas only pressure is enforced on the boundaries of the voids. For zero volume connections, no forces are added.

These forces are computed from the balance of momentum of the fluid. Let us denote by  $f_t$  the tangential forces per unit length of the channel acting on to the fluid (the opposite of the tangential forces acting on to the grains). The balance of momentum equation for the fluid reads:

$$\frac{dp}{ds} + f_t = 0, \quad (37)$$

where  $-f_t/2$  are the tangential forces prescribed on the boundaries of the two grains defining the studied channel. In this paper, for simplicity, Eq. 37 is written with the true pressure. In fact, only the gradient of the non-gravity part of the pressure should be used here. The simplification done is rigorous for a horizontal computation. For other cases, it has to be considered as an approximation. It should not be difficult to use an exact equation instead of Eq. 37.

### 3.5 Constitutive equation of the grains

The grains are assumed to be hyperelastic. In the following, the finite elastic “Neo-Hookean” model is assumed for constitutive equation of the solid constituents. It can be written:

$$\sigma_{mk}^\alpha = \frac{\mu}{J^{0\alpha}} (b_{mk}^{0\alpha} - \delta_{mk}) + \frac{\lambda}{J^{0\alpha}} (\ln J^{0\alpha} \delta_{mk}), \quad (38)$$

where  $\sigma_{mk}$  is the Cauchy stress tensor,  $b_{mk}^{0\alpha}$  the left Green Lagrange strain tensor,  $\delta_{mk}$  the unit tensor,  $\alpha$  denotes the time corresponding to the current configuration, 0 the corresponding reference one and  $J^{0\alpha}$  in the determinant of  $b_{mk}^{0\alpha}$ .  $\lambda$  and  $\mu$  the Lamé coefficients of the model.

### 3.6 Constitutive equations of the cohesive interfaces

Such a constitutive relation gives the force  $T$  as a function of the history of the relative displacement  $\Delta$  on the interface. For this first approach, a simple constitutive equation has been assumed for the interfaces. The normal component of the force  $T_n$  is assumed to depend only on the

history of the normal component of the relative displacement  $\Delta_n$ . A similar relation is assumed to hold for the tangential components  $T_t$  and  $\Delta_t$ . This means a decoupling between the normal and the tangential component of the forces. Both constitutive relations are assumed to be simple damage laws with a linear elastic step followed by a damage linear softening branch if the interface is loaded monotonically like it is sketched in Fig. 2. If the relative displacement exceeds a given value ( $\delta_n$  or  $\delta_t$  depending on the studied part of the constitutive equation), then the link between the two grains is completely broken and the forces are set equal to zero. This describes the tangential behavior independently on the sign of the relative displacement and the normal behavior in the case of opening. In the case of closure, the relative displacement cannot be negative and we enforce with a unilateral boundary condition.

The approach proposed in this paper can be easily generalized to any complex interface laws like the ones developed by Needleman [25] or Tvergaard [31].

### 3.7 Constitutive equations of the fluid

The first one correspond to the isotropic part of this constitutive equation:

$$\dot{q} = \frac{q}{k^w} \dot{p}^t. \quad (39)$$

It applies for the channel and for the voids. The differential Eq. (39) can be integrated as:

$$q = q_0 \exp\left(\frac{1}{k^w}(p - p_0)\right). \quad (40)$$

The second one, which is related to the viscosity of the fluid, can be obtained by integrating the Navier-Stokes equation for a channel. It gives the flux as a function of the gradient of pressure.

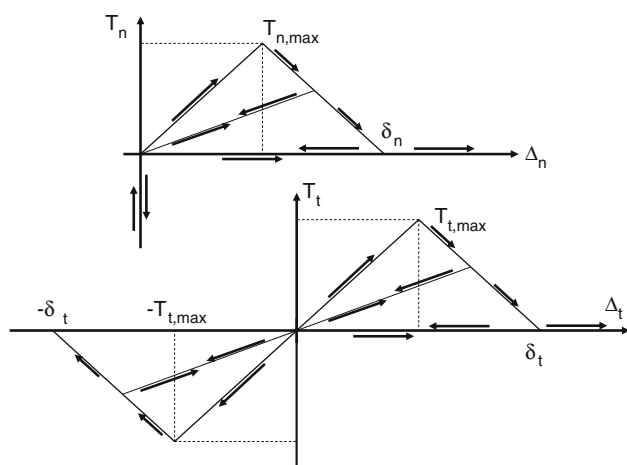


**Fig. 2** Constitutive equation of the interface

$$\frac{\overline{q}}{q} = \kappa \frac{dp}{ds}, \quad (41)$$

where  $\kappa$  depends on the viscosity but also on the opening and the shape of the channel, related to the opening of the cohesive interface. This dependence allows us to consider different assumptions according to the expected shape of the channels. In order to compute  $\kappa$  at all integration point, equations of Stokes are reduced and solved in each channel with simplifying assumptions.

It is necessary to integrate the differential equation (41), in the form:

$$p'(s) = \frac{1}{\kappa(s)q_0 \exp(1/k^w(p(s) - p_0))} \overline{q}, \quad (42)$$

where  $\overline{q}$  is constant and  $\kappa(s)$  is known. Finally, we end up with a relation linking the difference of the pressure between the two ends of the studied channel and the mass flux  $\overline{q}$  crossing this channel.

This equation can be integrated using the following method. It is a separable ordinary equation that can be recast as:

$$p'(s) \exp\left(\frac{1}{k^w}p(s)\right) = \frac{1}{\kappa(s)} \frac{\exp(1/k^w p_0)}{q_0} \overline{q}. \quad (43)$$

Let us denote by  $i$  and  $j$  the values of  $s$ , respectively, at one end and at the other end of the studied channel. By integrating Eq. (43), we get:

$$\begin{aligned} k^w \left( \exp\left(\frac{1}{k^w}p(j)\right) - \exp\left(\frac{1}{k^w}p(i)\right) \right) \\ = \left( \frac{\exp(1/k^w p_0)}{q_0} \int_i^j \frac{1}{\kappa(s)} ds \right) \overline{q}. \end{aligned} \quad (44)$$

If the function  $\kappa(s)$  is known, which means if the opening of the interfaces is known, then we can use a classical Gauss quadrature formulae in order to compute  $\int_i^j 1/\kappa(s) ds$ . We end up with a non-linear relation between  $\overline{q}$  and the values of the pressure at the ends of the channel.

### 3.8 Solution of the problem at the microscale

Due to the physical assumption at the microscale, the equations corresponding to the fluid network have a simple form. After spatial discretization, they correspond only to interfaces whereas the mechanical equations are written for the grains discretized by finite elements. Contrary to what has been done at the macroscopic scale, it is more convenient to solve the equations of the mixture by splitting them into the ones corresponding to the deformations of the grains and the other ones for the fluid network in the spirit of what has been done in [13, 23, 28] for instance.



In order to well understand the following, let us detail the forces acting on two grains joined by an interface. This is sketched in Fig. 3. On a given contact point between two grains, the forces due to the interface on grain 1 are given by normal  $T_n$  and tangential  $T_t$  components, whereas the forces acting on grain 2 are  $-T_n$  and  $-T_t$ , they are drawn with solid lines. At the same point, the forces due to the fluid acting on grain 1 are  $F_p$ , due directly to the pressure, and  $t$  defined in Eq. 37, whereas the forces acting on grain 2 are  $-F_p$  and  $t$ , drawn with dashed lines.

The non-linear equations are solved iteratively. A first guess is assumed for the problem which means that the position of all the points of the grains, the opening the interface, the pressure field inside the channel are assumed to be known. The pressure field of the fluid is then frozen and the non-linear mechanical problem is solved iteratively. The opening of the interface induces only change in the forces  $T_n$  and  $T_t$  for every point of the interface. After convergence of the mechanical problem, the opening of the channel have changed, inducing some changes of functions  $\kappa(s)$ . Then freezing these openings, the fluid equations are solved to get a new pressure field. This procedure is reiterated up to convergence.

This algorithm is summarized in the Table 1.

Item 3 in the Algorithm 1 is solved using a classical non-linear finite element method by a Newton–Raphson method and a proper linearization of the non-linear equations.

Item 5 is less classical, it is then necessary to detail the method. After solving the ordinary differential Eq. (42) for every interface (channel), we have (see Eq. 44) a relation giving the flux percolating in a channel as a function of the difference between the exponential of the pressures at both end of the studied channel. Let us assume that we have an hydraulic network of  $N$  voids (nodes like  $A, B, DCFG$  for

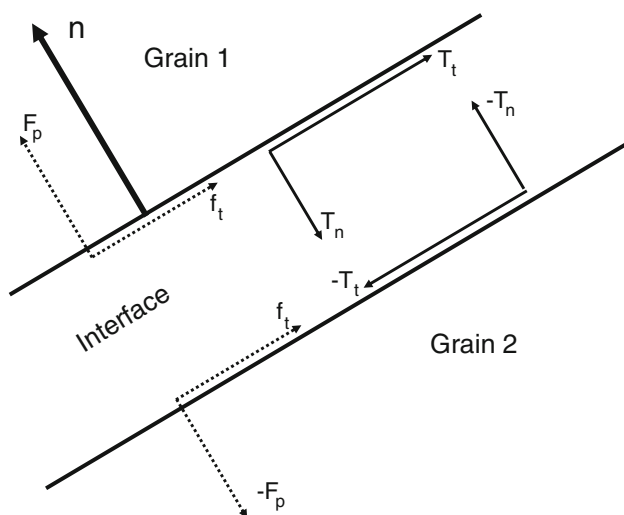


**Fig. 3** Forces acting on the boundaries of two grains

**Table 1** Algorithm at the microscale

1. Initial configuration corresponding to the start of the step: coordinates of point of the grains, opening of the interface, pressure along the channels, which allows to know the forces due to the fluid acting on the grains.
2. Assumption on the final configuration (coordinates and opening) and the final pressure
3. Solving the mechanical non-linear problem by a classical iterative procedure:
4. Update coordinates and opening and compute functions  $\kappa(s)$
5. Solving the fluid network
6. Update the pressure and compute the forces due to the fluid acting on the grains
7. Check the accuracy of the computed solution
  - If convergence: go to 8
  - If no convergence: go to 3
8. End of the step

instance in Fig. 1) and  $n$  channels (like  $AB, BC, HA$  for instance). The unknowns are the  $n$  fluxes  $\bar{w}$  in every channel the  $N$  pressures of the voids and the pressure of the  $v$  points of the network belonging to the boundary of the R.E.V. (like  $M, M', I$  and  $I'$  for instance). Let us notice that in fact we obtain first a system of equations for which the unknowns are for every void  $\exp(1/k^w p)$  where  $p$  is the pressure inside the void. In order to solve the problem, we have  $N$  equations like Eq. (36) and  $n$  equations like Eq. (44).

### 3.9 Boundary conditions for the REV

There are different approaches to transmit the macroscopic loadings on the REV. It is known that the more efficient one is the use of periodic conditions. The formulation is classical for the mechanical part. The difference of the position of two homologous points ( $M$  and  $M'$  or  $I$  and  $I'$  in the  $x$  direction for instance, see Fig. 1) has to meet the kinematical condition (see [3] for the details).

For the fluid, it is assumed similarly that the difference between the pressures of two homologous points is given by the macroscopic gradient of pressure. For instance, the difference between the pressure of  $M$  and  $M'$  or  $I$  and  $I'$  are taken as the  $x$  component of the gradient of the pressure at the macroscale. Moreover, the mass fluxes of two homologous points are enforced to be equal. It is also necessary to enforce the value of the mean value of the pressure in the R.E.V., otherwise the system of equations is singular. This is achieved using an iterative procedure. In a first iteration, the pressure is enforced in a point of the boundary of the R.E.V., the fluid equations are solved, then the new mean pressure is computed and the boundary pressure is then change of the difference between the intended mean value

and the computed one. This is iterated until convergence, which is usually very fast.

### 3.10 Computation of the macroscopic response

Let us assume now that the process described in the Algorithm 1 has converged. The computation gives  $\sigma_{il}$ ,  $q^{\text{mix}}$ ,  $\dot{M}$  and  $m_i$ . The consistent tangent stiffness matrix is obtained by finite differences using the computed values of these quantities.

- The stress  $\sigma_{il}$  is obtained as average of microscopic stress values. If there is some void, it is necessary to take into account the fluid part.
- $q^{\text{mix}}$  is also obtained as average over the REV.
- In order to obtain  $\dot{M}$ , it is necessary to divide by the time step, the difference between the values of  $M$  at the beginning and at the end of the time step.
- $m_i$  is obtained by averaging of *oriented* values of the fluxes  $\bar{\omega}$ .

## 4 One dimensional example

We consider a one-dimensional geometry composed by 3 elastic grains of length  $l^1$ ,  $l^2$  and  $l^3$  separated by cohesive interfaces filled up by fluid of pressure  $p^1$  and  $p^2$  respectively (Fig. 4).

The 1D structure is loaded through an applied displacement  $u^5$  and the interface fluid pressures  $p^1$  and  $p^2$ .

Equilibrium at points 1, 2, 3 and 4 is written as:

$$\begin{aligned} \sigma_1^1 - T_1^1 - p^1 &= 0 & \sigma_1^1 &= \sigma_1^2 = \sigma_1^3 \\ -\sigma_1^2 + T_1^1 + p^1 &= 0 & \text{leading to : } T_1^1 + p^1 &= T_1^2 + p^2 \\ \sigma_1^2 - T_1^2 - p^2 &= 0 & \sigma_1^1 - T_1^1 - p^1 &= 0 \\ -\sigma_1^3 + T_1^2 + p^2 &= 0 \end{aligned}$$

The elastic behavior of the grains gives:

$$\frac{u^1}{l^1} = -K^1 \sigma_1^1; \quad \frac{u^3 - u^2}{l^2} = -K^2 \sigma_1^2; \quad \frac{u^5 - u^4}{l^3} = -K^3 \sigma_1^3$$

The behavior of the cohesive interfaces is may be classified as:

Elastic	Softening	Unloading	Failure
$u^2 - u^1 = -k^1 T_1^1$	$u^2 - u^1 = -k'^1 T_1^1 + \delta_c^1$	$u^2 - u^1 = -k''^1 T_1^1$	$T_1^1 = 0$
$u^4 - u^3 = -k^2 T_1^2$	$u^4 - u^3 = -k'^2 T_1^2 + \delta_c^2$	$u^4 - u^3 = -k''^2 T_1^2$	$T_1^2 = 0$

where  $k'^1 = k^1$  and  $k''^2 = k^2$  constant if unloading occur during elastic phase.

Considering the 4 phases of the interfaces behavior, the resolution of the equilibrium system leads to 7 solutions: 3 symmetrical solutions (in which interfaces 1 and 2 follow the same behavior) and 4 non-symmetrical solutions (different behavior for interfaces 1 and 2).

- Symmetrical solutions :

*interface 1 : load; interface 2 : load*

$$\sigma_1^1 = \frac{-(1/k^1)u^5 + (k^2/k^1)p^2 + p^1}{1 + (K^1 l^1 + K^2 l^2 + K^3 l^3 + k^2)/k^1}$$

*interface 1 : softening; interface 2 : softening*

$$\sigma_1^1 = \frac{-(1/k^1)u^5 + (k^2/k^1)p^2 + (1/k'^1)\delta_c^2 + (1/k'^1)\delta_c^1 + p^1}{1 + (K^1 l^1 + K^2 l^2 + K^3 l^3 + k^2)/k^1}$$

*interface 1 : failure; interface 2 : failure*

$$\sigma_1^1 = p^1 = p^2$$

- Non-symmetrical solutions :

*interface 1 : unload; interface 2 : softening*

$$\sigma_1^1 = \frac{-(1/k'^1)u^5 + (k^2/k'^1)p^2 + (1/k'^1)\delta_c^2 + p^1}{1 + (K^1 l^1 + K^2 l^2 + K^3 l^3 + k^2)/k'^1}$$

*interface 1 : softening; interface 2 : unload*

$$\sigma_1^1 = \frac{-(1/k'^1)u^5 + (k'^2/k^1)p^2 + (1/k^1)\delta_c^1 + p^1}{1 + (K^1 l^1 + K^2 l^2 + K^3 l^3 + k'^2)/(k^1)}$$

*interface 1 : unload; interface 2 : failure*

$$\sigma_1^1 = p^2$$

*interface 1 : failure; interface 2 : unload*

$$\sigma_1^1 = p^1$$

### 4.1 Verification

In order to compare with the obtained analytical solutions, we consider numerical computations with mechanical loading  $F_{11} = 1 + 0.02(*\alpha)$  (loading factor  $\alpha$ ) corresponding to displacement  $u_5 = 0.02(*\alpha)$ , and fluid pressure  $p_1 = p_2 = p$ .

Parameters used for numerical and analytical models are:

	Numerical elastic model	Analytical elastic model	Cohesive interfaces model
$E$	3460.68 MPa	$K_1 = K_2$	$2.6 \cdot 10^{-4}$ MPa $\alpha^{-1}$
$\nu$	0.2	-	$T_{max}$
			$\delta_c = \delta_n$
			0.015 mm
			5 MPa

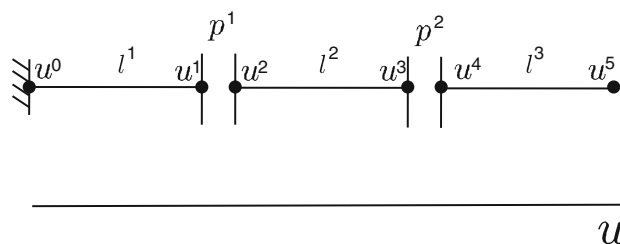


Fig. 4 1D geometry with 2 cohesive interfaces

Modulus  $K_1$  is computed with respect to the generalized Neo-Hookean law under periodic uniaxial conditions ( $\epsilon_{22} = \epsilon_{33} = 0$ ):

$$\frac{1}{K_1} = \frac{E}{1+\nu} \left( 1 + \frac{\nu}{1-2\nu} \right) \quad (45)$$

On Fig. 5, we compared analytical and numerical solutions for two different loading cases. In the first case, a pure mechanical loading is applied, and in the second case, a mixed loading with average fluid pressure  $p_1 = p_2 = p = 4.0\alpha$  MPa. We observe that numerical symmetrical and non-symmetrical solutions match analytical ones for the different phases of the cohesive interfaces behavior.

## 5 Numerical examples

The objective of the present paper is to illustrate the macroscopic poro-elastic damage response resulted from the numerical homogenization scheme. The main features of this response result from the analysis of the local macroscopic behavior and this point will be illustrated through following numerical examples. Such a computed behavior may be used, in a two-scale algorithm, at each Gauss point of a macroscopic FEM computation. Although this is beyond the objective of the present contribution, we gave

details about how this integration could be done within a FE<sup>2</sup> framework in Sect. 2.3.

Verification have been done using particular one-dimensional problems for which analytical solutions are available (see [15]). Moreover, the results obtained in the particular case of uncoupled problems have been successfully compared with the computations of Bilbie et al. [3].

In order to completely validate the method, the following R.E.V. given in Fig. 6 is used at the microlevel. The finite element mesh used for the grains, and the numbering of the interfaces can be seen in Fig. 6.

The mechanical parameters used are detailed in the Table 2.

For the computations presented hereafter, the transformation gradient, the mean pressure, and the pressure gradient (which in a real computation come from the macro calculations) are here defined as a function of  $\alpha$ , which is the time. The evolutions of the mean stress and the fluid mass flow are then presented as functions of this time. Our method gives a direct quantification of the link damage/ fluid mass flow, as compared with the analytical approaches, since it accounts for complex failure patterns and the associated fluid flow at the microscale.

Four different computations are presented in the following. Two computations use a simple loading scheme: first a loading path where only the pressure increases is detailed, then a loading path for which both the kinematics

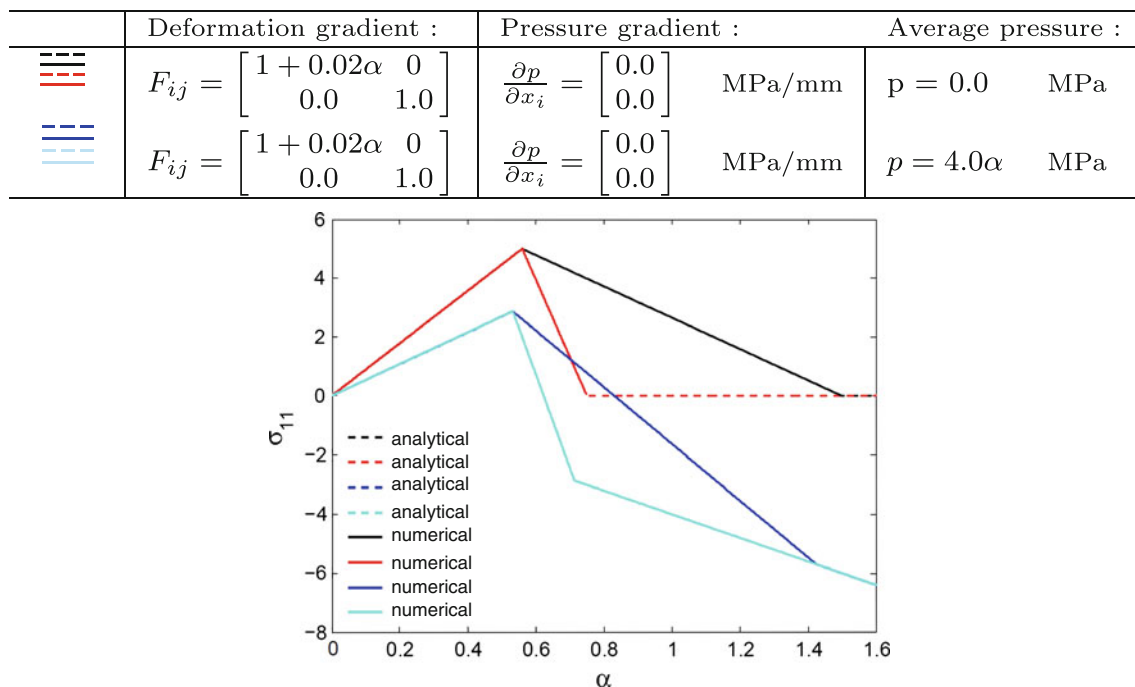


**Fig. 5** Stress evolution  $\sigma_{11}$  (MPa), 1D verification for two average pressures

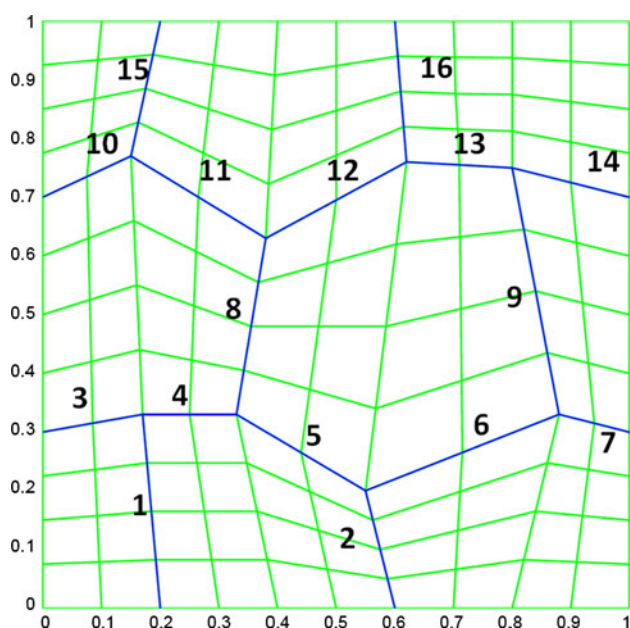


**Fig. 6** R.E.V geometry and interfaces numbers

and the pressure evolve is studied. Finally, the last computations use a more complex loading in two steps: first part with hydraulic or mixed loading, second part with applied gradient of pressure.

### 5.1 Influence of the mean fluid pressure

In this first example, the loading path is defined as follows:  $F_{ij}$  is kept constant, equal to the identity. The pressure gradient is kept constant and equal to 0. The mean pressure starts with a zero value and increases linearly with  $\alpha$  up to 100 MPa. The evolutions of the stress components of the mixture are given in Fig. 7 as functions of  $\alpha$ . The states of the R.E.V., for three different values of  $\alpha$  shown in Fig. 7, are given in Fig. 8. A red triangle indicates a point for which the damage process has begun in the normal direction (i.e. points in the softening regime, which means  $0.33 \leq \Delta u_n \leq 1$ ). A red circle denotes a point completely broken in the normal direction (i.e.  $\Delta u_n \geq 1$ ) and a black star indicates that the corresponding point of the interface is closed due to compressive forces.

In Fig. 7, it can be seen that the shear stress does not evolve. On the contrary, the other components of the mean

stress increase linearly up to  $\alpha = 0.46$  a state corresponding to the beginning of softening of some interfaces. Then, the evolution depends on the opening of the channels and of the fact that, due to a global zero deformation, the increase in the stress inside the grains depends on the details of the geometry of the grains in the R.E.V.

Figure 8 shows clearly the rupture of the R.E.V. due to the increase in the pressure. Fluid pressure act like mechanical tractions on the cohesive interfaces and consequently the damaged state of the interfaces is directly link with the pressure distribution in the interfaces. This rupture is localized and a layer of interface more or less normal to the  $y$  direction is highly damaged. On the contrary, a side effect is a tendency of closure for the other layer of interfaces.

### 5.2 Mixed loadings

Three loading paths differing only by the value of the final mean fluid pressure are applied to the R.E.V. The deformation gradient (starting from identity) is increasing up to:

$$F_{ij} = \begin{bmatrix} 1.02 & 0 \\ -0.02 & 1.01 \end{bmatrix}. \text{ This means that there is both}$$

straining in the  $x$  and  $y$  directions but also shear straining. The pressure gradient starts with a zero value and increases linearly with  $\alpha$  up to 0.1 MPa/mm. The mean pressure increases up to three different values corresponding to the three different computations, namely: 5, 15 and 30 MPa.

The evolutions of the stress components of the mixture for the three cases are given in Fig. 9 as functions of  $\alpha$ . Let us notice that the evolutions of the components of the mixture stress are not necessarily monotonic. This is clearly an effect of the interface behavior, especially of the possible softening of the forces transmitted by the interfaces.

The states of the R.E.V. for three different values of  $\alpha$  and for only two of the three cases, namely for 5 MPa in the first row of the picture and for 30 MPa for the second row of the picture are given in Fig. 9 (the corresponding states are indicated in Fig. 10). The same symbols as for the previous case are taken in order to describe the state of the damage in every point of the interfaces. It has been found interesting to consider only the damage in the normal direction. Even if the damage depends clearly on the level

**Table 2** Parameters of the models

Elastic model of the grains			Interface model			Fluid properties		
$\lambda$	961.0	MPa	$\delta_n$	0.015	mm	$\nu$	$10^{-9}$	MPa s
$\mu$	1442.0	MPa	$\delta_t$	0.015	mm	$\rho_0$	$10^{-3}$	g/mm <sup>3</sup>
$\rho$	$2.7 \times 10^{-3}$	g/mm <sup>3</sup>	$T_{n,\max}$	5.0	MPa	$p_0$	0.1	MPa
			$T_{t,\max}$	5.0	MPa	$k_w$	$2.2 \times 10^3$	MPa

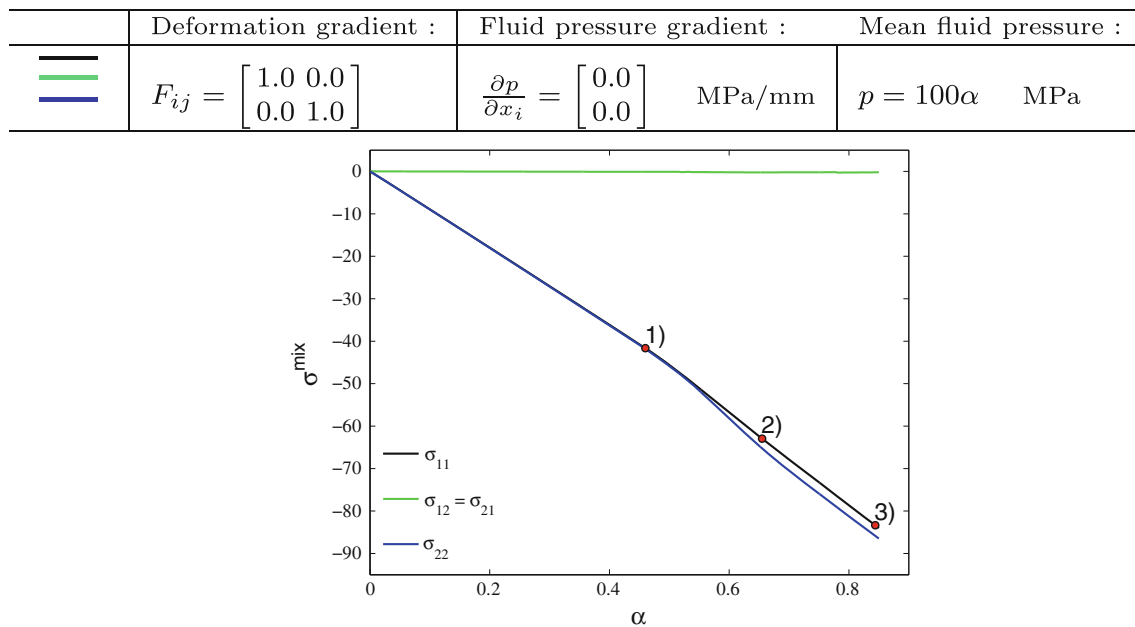


**Fig. 7** Mixture stress evolution  $\sigma^{\text{mix}}$  (MPa) under mean fluid pressure loading

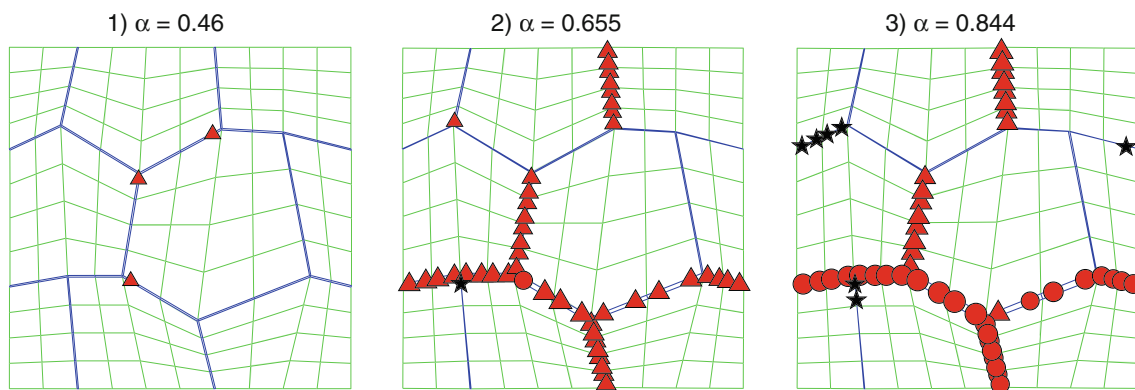


**Fig. 8** Deformed R.E.V and interface states under mean fluid pressure loading (Fig. 7) for three different times; *red triangle* point in the softening regime, *red circle* broken points, *black star* point closed again due to compressive forces (colour figure online)

of the fluid pressure, the degradation schemes are clearly similar and seem to be governed in this case mainly by the kinematics prescribed on the R.E.V.








The evolution of the mass fluxes of fluid, in direction 1 (on the left) and in vertical direction 2 (on the right hand side), are drawn in Fig. 11. In the early stages, both curves evolve with the increase in the pressure gradient and the elastic opening of the interfaces. On the contrary, the ultimate stages show an increase of the mass fluxes very different due to the decohesion of some parts of the interfaces. This effect is particularly clear for the case corresponding to the higher pressure 30 MPa. However, these curves are not monotonous showing the complexity of the evolution of the R.E.V. as some points are finally completely closed inducing a decreasing of the fluid fluxes

even if the pressure gradient increases. For instance, the fact that interface numbered 4 in Fig. 6 is elastically loaded, then unloaded close to closure explains the decreasing of the fluxes in direction 2.

This decrease of the fluid mass flow illustrated the effect of the progressive closure of the interfaces on the fluid part. As detailed in the previous part, the fluid mass flow is computed with respect of the normal opening of the interfaces (power of 3), consequently it decrease during the closure process of the interface. On the mechanical side, the closure of the interface follow the linear unloading part of the cohesive law 3.6.

In order to well understand these results, it is interesting to relate the evolutions of the properties of the R.E.V. with the damage states as they are partially depicted in Fig. 10.



	Deformation gradient :	Fluid pressure gradient :	Mean fluid pressure :
	$F_{ij} = \begin{bmatrix} 1 + 0.02\alpha & 0 \\ -0.02\alpha & 1 + 0.01\alpha \end{bmatrix}$	$\frac{\partial p}{\partial x_i} = \begin{bmatrix} 0.1\alpha \\ 0.1\alpha \end{bmatrix}$ MPa/mm	$p = 5\alpha$ MPa
			
	$F_{ij} = \begin{bmatrix} 1 + 0.02\alpha & 0 \\ -0.02\alpha & 1 + 0.01\alpha \end{bmatrix}$	$\frac{\partial p}{\partial x_i} = \begin{bmatrix} 0.1\alpha \\ 0.1\alpha \end{bmatrix}$ MPa/mm	$p = 15\alpha$ MPa
			
	$F_{ij} = \begin{bmatrix} 1 + 0.02\alpha & 0 \\ -0.02\alpha & 1 + 0.01\alpha \end{bmatrix}$	$\frac{\partial p}{\partial x_i} = \begin{bmatrix} 0.1\alpha \\ 0.1\alpha \end{bmatrix}$ MPa/mm	$p = 30\alpha$ MPa
			
			

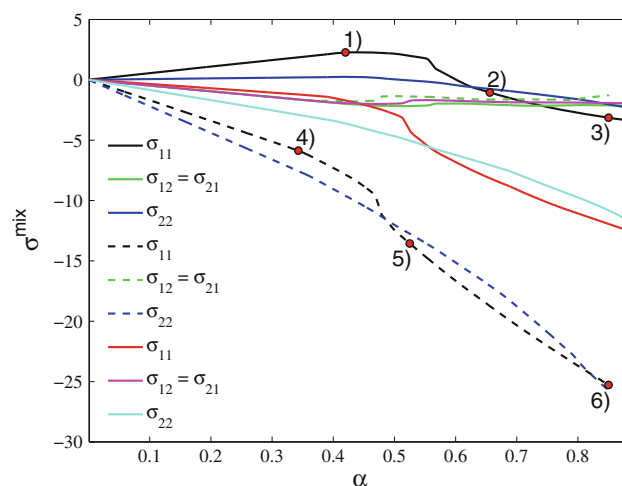


**Fig. 9** Mixture stress evolution  $\sigma^{\text{mix}}$  (MPa) under mixed loading

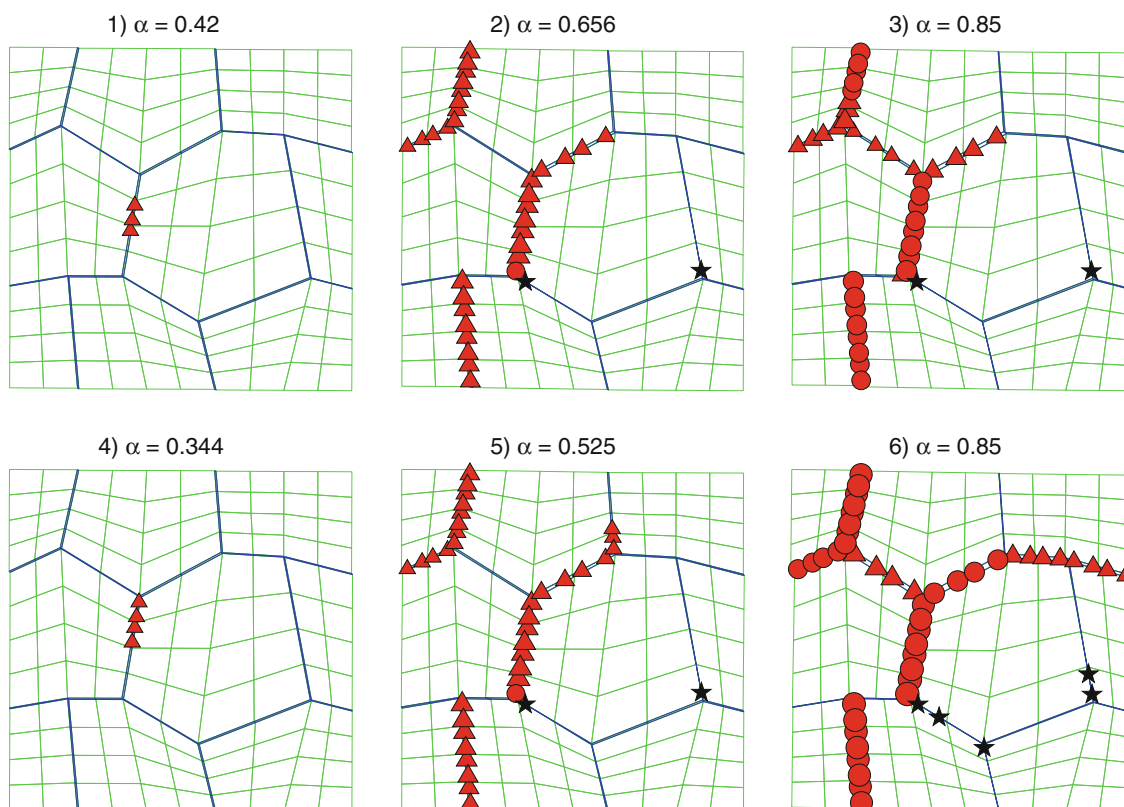


**Fig. 10** Deformed R.E.V and interface states under mixed loading (Fig. 9); red triangle point in the softening regime, red circle broken points, black star point closed again due to compressive forces (colour figure online)

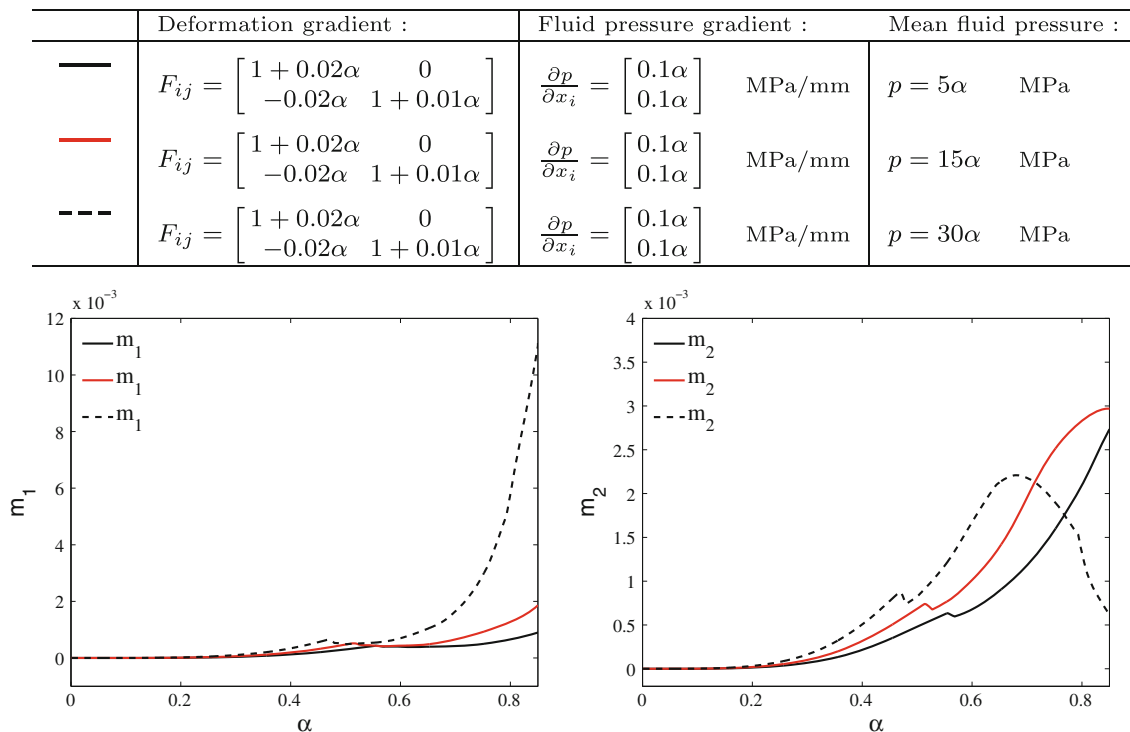


**Fig. 11** Mass flux evolution  $m_i$  (g/s) under mixed loading

### 5.3 Complex loadings

For these last simulations, more complex loadings are considered in which the loading process consists of two steps:

- Loading 1:** a hydraulic or mixed loading path is applied,
- Loading 2:** gradient of pressure is applied.

The influence of the average damage level of the R.E.V. on the fluid circulation is studied. Two cases are represented: In the first case, the fluid mass flux evolution in a *intact* R.E.V. is compared to the fluid mass flux evolution in a R.E.V. *damaged* by hydraulic loading. In the second case, the fluid mass flux evolution in a *intact* R.E.V. is compared to the fluid mass flux evolution in a R.E.V. *damaged* by mixed loading.

#### 5.3.1 Hydraulic loading

During the first part of the loading process, an average pressure of  $\alpha$  100 MPa is applied (no gradient of pressure). At  $\alpha = 0.1$ , we define the *intact* R.E.V. state (Fig. 12) in which no interfaces are damaged. At  $\alpha = 0.8$ , interfaces of the bottom part are broken, this state defines the *damaged* R.E.V. After reaching the intact or damaged state, the pressure is kept constant and we start to apply a pressure gradient up to 0.1 MPa/mm in both directions in order to observe the mass flux evolution starting from *intact* or *damaged* R.E.V.

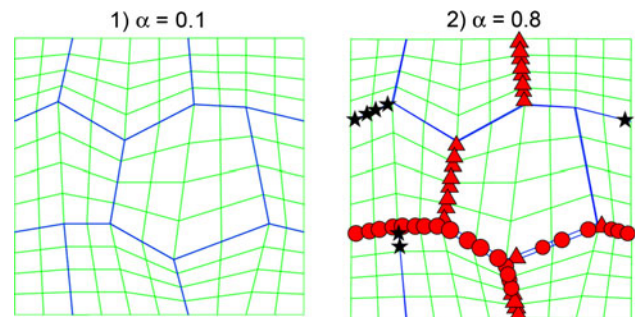


**Fig. 12** *Intact* R.E.V and *damaged* R.E.V under hydraulic loading (Figs. 14, 15); red triangle point in the softening regime, red circle broken points, black star point closed again due to compressive forces (colour figure online)

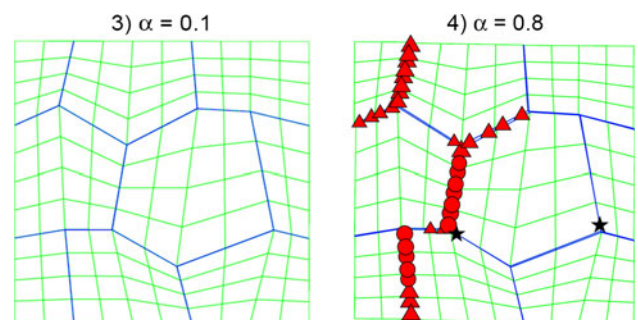


**Fig. 13** *Intact* R.E.V and *damaged* R.E.V under mixed loading (Figs. 14, 15); red triangle point in the softening regime, red circle broken points, black star point closed again due to compressive forces (colour figure online)

	Loading 1 :		Loading 2 :
	Deformation gradient :	Mean fluid pressure :	Fluid pressure gradient :
—	$F_{ij} = \begin{bmatrix} 1.0 & 0.0 \\ 0.0 & 1.0 \end{bmatrix}$	$p = 100\alpha$ MPa	$\frac{\partial p}{\partial x_i} = \begin{bmatrix} 0.1\alpha \\ 0.1\alpha \end{bmatrix}$ MPa/mm
—	$F_{ij} = \begin{bmatrix} 1 + 0.02\alpha & 0 \\ -0.02\alpha & 1 + 0.01\alpha \end{bmatrix}$	$p = 5\alpha$ MPa	$\frac{\partial p}{\partial x_i} = \begin{bmatrix} 0.1\alpha \\ 0.1\alpha \end{bmatrix}$ MPa/mm

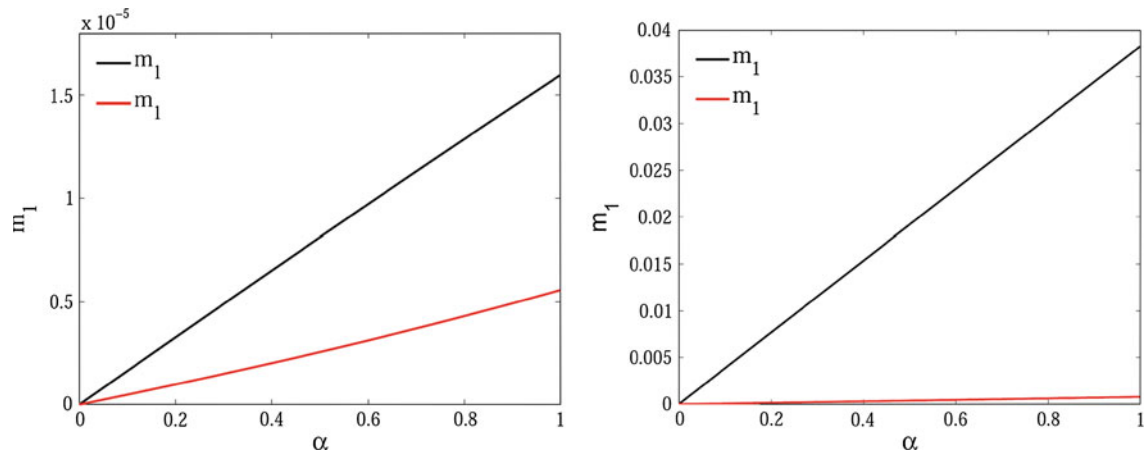


**Fig. 14** Horizontal mass flux evolution  $m_1$  (g/s) for *intact* R.E.V (left) and *damaged* R.E.V (right) under hydraulic and mixed loading

	Loading 1 :		Loading 2 :
	Deformation gradient :	Mean fluid pressure :	Fluid pressure gradient :
—	$F_{ij} = \begin{bmatrix} 1.0 & 0.0 \\ 0.0 & 1.0 \end{bmatrix}$	$p = 100\alpha$ MPa	$\frac{\partial p}{\partial x_i} = \begin{bmatrix} 0.1\alpha \\ 0.1\alpha \end{bmatrix}$ MPa/mm
—	$F_{ij} = \begin{bmatrix} 1 + 0.02\alpha & 0 \\ -0.02\alpha & 1 + 0.01\alpha \end{bmatrix}$	$p = 5\alpha$ MPa	$\frac{\partial p}{\partial x_i} = \begin{bmatrix} 0.1\alpha \\ 0.1\alpha \end{bmatrix}$ MPa/mm

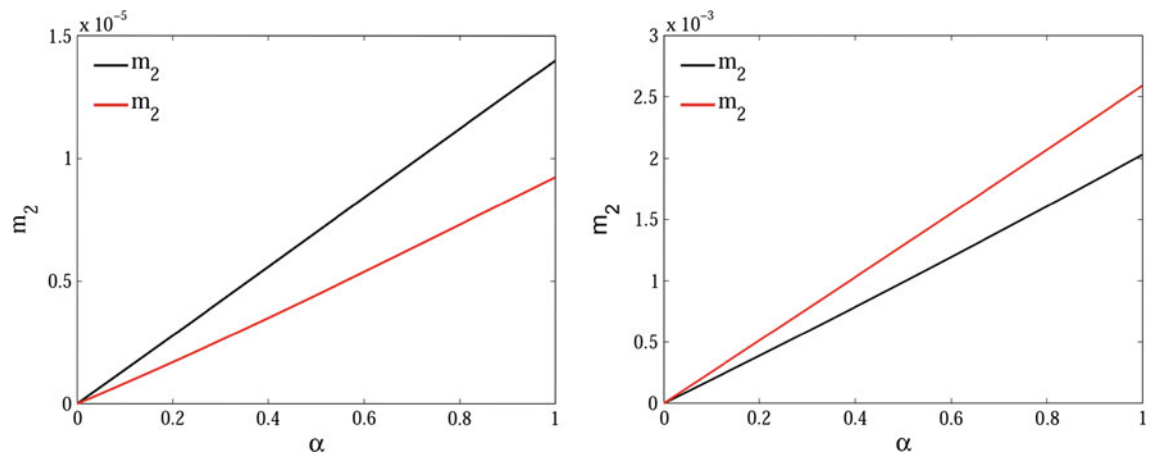


**Fig. 15** Vertical mass flux evolution  $m_2$  (g/s) for *intact* R.E.V (left) and *damaged* R.E.V (right) under hydraulic and mixed loading

### 5.3.2 Mixed loading

For the mixed loading, the first loading part is composed of a gradient of deformation and an average fluid pressure  $\alpha$

5 MPa (no gradient of pressure). At  $\alpha = 0.1$ , the *intact* R.E.V. state is defined (Fig. 13). At  $\alpha = 0.8$ , two interfaces of the left side reach total decohesion. This state defines the *damaged* R.E.V. Starting for intact or damaged R.E.V., the

previous mixed loading path is then blocked and the gradient of pressure is increased linearly up to 0.1 MPa/mm.

### 5.3.3 Mass flux evolution

On Figs. 14 and 15, the evolution of the components of the fluid mass flux are compared for the two complex loading previously described. The components of the mass flux evolve linearly with the increase in the pressure gradient. We observe in Fig. 14 that, in both loading cases, the horizontal mass flux is much stronger in the *damaged* R.E.V. ( $\sim 10^3$ ) than in the *intact* R.E.V. In the hydraulic loading case, the corresponding state of the damaged R.E.V. show that horizontal interfaces are broken, so the fluid can freely circulate in this direction. In the mixed loading case, horizontal interfaces are not damaged (normal opening of these interfaces is too small), moreover some of them are unloading (interface number 5 is re-closed). With this decohesion scheme, the fluid is not able to circulate easily and consequently the mass flux is lower than the mass flux obtained under hydraulic solicitations.

On the vertical component in Fig. 15, the same observations on the fluid mass flux magnitude are made. The mass flux is  $\sim 10^2$  bigger in the damaged R.E.V. Regarding the two loading cases, the mass flux with mixed loading path is stronger because vertical interfaces are opened. This decohesion scheme facilitate the vertical fluid circulation.

## 6 Concluding remarks

A two-scale computational homogenization scheme for poro-mechanical damage has been proposed. Granular microstructures with (hyper)elastic grains separated by cohesive interfaces filled with fluid have been considered. The numerical upscaling procedure has been described in detail, and the resulting homogenized behavior is illustrated on a number of numerical tests.

The results revealed the strong coupling between damage and transmissivity properties of the homogenized model, dependent on the loading path. It has been showed that the proposed approach is able to describe complex behaviors, very difficult to model with phenomenological constitutive relations, like those resulting from the re-closure of the interfaces after inter-granular failure.

It is important to note that, in the present approach, there is no need to define the effective stresses which definition to some extent is controversial. The essential assumptions concerning the hydro-mechanical coupling are done at the level of the microstructure, where an explicit interaction between the fluid, the solid grains, and the cohesive interfaces is assumed.

By pushing the phenomenological assumptions down-scale, the explicit description of the microstructure is obtained and provides a better understanding of the phenomena at the small scale. For example, the macroscopic failure due to partial grain decohesion, contact and closure of interfaces and the associated fluid behaviors, cannot be modeled with classical approaches. Even if two-scale computations are time consuming, the approach is able to model with more physical refinement the geomechanical problems.

**Acknowledgments** The authors would like to acknowledge the French National Agency for Radioactive Waste Management ANDRA for its financial support.

## References

- Andrade JE, Borja RI (2007) Modeling deformation banding in dense and loose fluid saturated sands. *Finite Element Anal Design* 43(5):361–383
- Auriault JL, Borne L, Chambon R (1985) Dynamics of porous saturated media, checking of the generalized law of Darcy. *J Acoust Soc Am* 77:1641–1650
- Bilbie GL, Dascalu C, Chambon R, Caillerie D (2008) Microfracture instabilities in granula solids. *Acta Geotech* 3:25–36
- Biot MA (1941) General theory of three-dimensional consolidation. *J Appl Phys* 12:155–164
- Borne L, Chambon R, Auriault JL (1985) Conforming finite element computations applied to spatially periodic harmonic Navier Stokes equations. *Int J Numer Meth Fluids* 5:685–707
- Bowen RM (1980) Incompressible porous media models by use of the theory of mixtures. *Int J Eng Sci* 18:1129–1148
- Colin F, Chambon R, Charlier R (2006) A finite element method for poro mechanical modelling of geotechnical problems using local second gradient models. *Int J Numer Meth Eng* 65:1749–1772
- Coussy O (1995) *Mechanics of porous continua*. Wiley, London
- de Boer R (2000) *Theory of porous media*. Springer, Berlin
- Deudé V, Dormieux L, Kondo D, Maghous S (2002) Micromechanical approach to nonlinear poroelasticity: application to cracked rocks. *J Eng Mech* 848–855
- Dormieux L, Kondo D (2007) Micromechanics of damage propagation in fluid-saturated cracked media. *Revue Européenne de Gnie Civil* 11(7-8):945–962
- Ern A, Meunier S (2009) A posteriori error analysis of Euler-Galerkin approximations to coupled elliptic-parabolic problems ESAIM. *Math Model Numer Anal (Modlisation Mathématique et Analyse Numrique)* 43(2):353–375
- Felippa C, Park K (1980) Staggered transient analysis procedures for coupled mechanical systems: formulation. *Comput Methods Appl Mech Eng* 24:61–111
- Feyel F, Chaboche JL (2000) FE<sup>2</sup> multiscale approach for modelling the elastoviscoplastic behaviour of long fibre SiC/Ti composite materials. *Comput Methods Appl Mech Eng* 183:309–330
- Frey J (2010) *Modélisation multi-échelles de l'endommagement hydro-mcanique des roches argileuses*, PhD Thesis Grenoble University, Grenoble
- Frey J, Chambon R, Dascalu C (2009) A two-scale poromechanical model, PORO-MECHANICS IV, 4th Biot conference on poromechanics, Columbia University, New York, pp 461–466
- Gatmiri B, Delage P (1997) A formulation of fully coupled thermal hydraulic mechanical behaviour of saturated porous

- media numerical approach. *Int J Numer Anal Meth Geomech* 21:199–225
18. Ghosh S, Lee K, Moorthy S (1994) Multiple scale analysis of heterogeneous elastic structures using homogenization theory and Voronoi cell finite element method. *Int J Solids Struct* 32:27–62
  19. Ghosh S, Lee K, Moorthy S (1995) Two scale analysis of heterogeneous elastic-plastic materials with asymptotic homogenization and Voronoi cell finite element model. *Comput Methods Appl Mech Eng* 132:63–116
  20. Hassanizadeh M, Gray W (1979) General conservation equations for multi-phase systems: 1. Average procedure. *Adv Water Res* 2:131–144
  21. Hassanizadeh M, Gray W (1979) General conservation equations for multi-phase systems: 2. Mass, moment, energy, and entropy equations. *Adv Water Res* 2:191–208
  22. Kouznetsova V, Geers MGD, Brekelmans WAM (2002) Multi-scale constitutive modelling of heterogeneous materials with a gradient-enhanced computational homogenization scheme. *Int J Numer Methods Eng* 54:1253–1260
  23. Lewis RW, Schrefler BA (1998) The finite element method in the static and dynamic deformation and consolidation of porous media. Wiley, New York
  24. Miehe C, Schroder J, Schotte J (1996) Computation homogenization analysis in finite plasticity simulation of texture development in polycrystalline materials. *Comput Methods Appl Mech Eng* 171:387–418
  25. Needleman A (1987) A continuum model for void nucleation by inclusion debonding. *J Appl Mech* 54:525–531
  26. Oden JT, Vemaganti K, Moës N (1998) Hierarchical modeling of heterogeneous media. *Comput Methods Appl Mech Eng* 172:3–25
  27. Ozdemir I, Brekelmans WAM, Geers MGD (2008) FE<sup>2</sup> computational homogenization for the thermo-mechanical analysis of heterogeneous solids. *Comput Methods Appl Mech Eng* 198:602–613
  28. Park K, Felippa C (1980) Partitioned transient analysis procedures for coupled field problems: accuracy analysis. *J Appl Mech* 47:919–926
  29. Simo JC, Taylor RL (1985) Consistent tangent operators for rate-independent elastoplasticity. *Comput Methods Appl Mech Eng* 48:101–118
  30. Smit RJM, Brekelmans WAM, Meijer HEH (1996) Prediction of the mechanical behavior of non linear heterogeneous systems by multi-level finite element modeling. *Comput Methods Appl Mech Eng* 155:181–192
  31. Tvergaard V (1990) Effect of fiber debonding in a whisker-reinforced metal. *Mater Sci Eng* 125:203–213